FEBS Letters 589 (2015) 3588–3594

FEBS Letters

journal homepage: www.FEBSLetters.org

Co-silencing of human Bub3 and dynein highlights an antagonistic relationship in regulating kinetochore–microtubule attachments

Patrícia M.A. Silva [a,b], Álvaro A. Tavares [b,c], Hassan Bousbaa [a,d,*]

[a] CESPU, Instituto de Investigação e Formação Avançada em Ciências e Tecnologias da Saúde, Rua Central de Gandra, 1317, 4585-116 Gandra PRD, Portugal
[b] Centre for Biomedical Research (CBMR), University of Algarve, Faro 8005-139, Portugal
[c] Departamento Ciências Biomédicas e Medicina, University of Algarve, Faro 8005-139, Portugal
[d] Centro Interdisciplinar de Investigação Marinha e Ambiental (CIIMAR/CIMAR), Universidade do Porto, Rua dos Bragas 289, 4050-123 Porto, Portugal

ARTICLE INFO

Article history:
Received 9 July 2015
Revised 3 October 2015
Accepted 15 October 2015
Available online 23 October 2015

Edited by Angel Nebreda

Keywords:
Bub3
Dynein
Spindly
Kinetochore–microtubule interaction
Chromosome congression
Antagonistic interaction

ABSTRACT

We previously reported that the spindle assembly checkpoint protein Bub3 is involved in regulating kinetochore–microtubule (KT-MT) attachments. Also, Bub3 was reported to interact with the microtubule motor protein dynein. Here we examined how this interaction contributes to KT-MT attachments. Depletion of Bub3 or dynein induced misaligned chromosomes, consistent with their role in KT-MT attachments. Unexpectedly, co-silencing of both proteins partially suppressed the misalignment phenotype and restored chromosome congression. Consistent with these observations, KT-MT attachments in co-depleted cells were stable, able to drive chromosome congression, and produce inter- and intra-kinetochore stretch, indicating they are functional. We suggest that a mutual antagonism exists between Bub3 and dynein to ensure optimal KT-MT attachments.

1. Introduction

Faithful chromosome segregation in mitosis relies on appropriate kinetochore–microtubule (KT-MT) attachments, under the surveillance of the spindle assembly checkpoint (SAC). The SAC prevents anaphase onset until all chromosomes accomplish proper bipolar attachments and come under tension. Core components of the SAC proteins include, among others, the evolutionary conserved Mad2, Bub3, and BubR1, which form the mitotic checkpoint complex (MCC) with Cdc20 whenever unattached or improperly attached kinetochores are present. As a consequence, Cdc20 is unable to activate the anaphase promoting complex/cyclosome (APC/C) and anaphase is blocked [1,2]. Besides this surveillance role, SAC components were also involved in the regulation of KT-MT attachments [3]. For instance, we previously reported that Bub3 is required for the establishment of stable end-on KT-MT attachments. Yet, the relationship between Bub3 and other proteins involved in the same process of KT-MT attachments remains unknown. A good candidate for this relationship is the cytoplasmic dynein. Dynein was reported to interact with Bub3 [4,5]. Although there is still no clear demonstration of a direct role of dynein in the formation of stable KT-MT attachments, in many reports, displacement of kinetochore dynein was reported to delay chromosome congression and the formation of load-bearing attachments. For instance, inhibition of dynein results in unstable KT-MT attachments and interferes with metaphase chromosome alignment [6,7]. Here, we studied the functional relationship between Bub3 and dynein in regulating KT-MT attachments.

2. Materials and methods

2.1. Cell culture and siRNA transfection

HeLa cells, HeLa cells stably expressing EGFP-Bub3 [8], and HeLa cells stably expressing EGFP-CENP-A (a gift from Dr. Lars Jansen, IGC, Lisboa, Portugal) were cultured in Dulbecco's Modified Eagle's Medium (DMEM, Biochrom, São Mamede de Infesta, Portugal), supplemented with 10% fetal bovine serum (FBS, Biochrom), and maintained at 37 °C, in a 5% CO_2 humidified atmosphere. For

Author contributions: HB conceived and designed the work. PS headed the experimental work and acquisition and analysis of data, and contributed to their interpretation. AT co-supervised the work and contributed to interpretation of data. PS and HB drafted the manuscript. All authors read, critically revised, and approved the final manuscript.

* Corresponding author at: Instituto de Investigação e Formação Avançada em Ciências e Tecnologias da Saúde, CESPU, 4585-116 Gandra PRD, Portugal.
E-mail address: hassan.bousbaa@iscsn.cespu.pt (H. Bousbaa).

http://dx.doi.org/10.1016/j.febslet.2015.10.017
0014-5793/

HeLa cell lines stably expressing EGFP-Bub3 and EGFP-CENP-A, the medium was supplemented with 400 μg/mL of a selective agent G418 and 1 μg/mL Blasticidin (Sigma–Aldrich Co., Saint Louis, MO, USA) respectively. For transfection with siRNAs, cells were seeded in 22 mm poly-L-lysine-coated coverslips in 6-well plates containing DMEM and, 24 h later, transfected using INTERFERin siRNA Transfection Reagent (PolyPlus, New York, USA) according to the manufacturer's instructions. The culture medium was replaced 6 h after transfection with fresh DMEM. Validated siRNA duplexes against Dynein Heavy Chain (DHC) and Bub3 (Santa Cruz Biotechnology, Dallas, USA) were used at a final concentration of 13.3 and 6.7 nM, respectively. A validated siRNA sequence against Spindly [9] was synthetized by Sigma–Aldrich and was used at a final concentration of 100 nM. Microscopic analysis was performed 48 or 72 h post-transfection.

2.2. Cell extracts and western blotting

For total cell extracts, cells were harvested by centrifugation and resuspended in lysis buffer (50 mM Tris pH 7.5; 150 mM NaCl; 1 mM EDTA; 1% Triton-100) containing a protease inhibitor cocktail (Sigma–Aldrich). Protein quantification was performed using a BCA™ Protein Assay Kit (Pierce Biotechnology), according to the manufacturer's instructions. A total of 15 μg of protein lysate was resuspended in SDS-sample buffer (375 mM Tris pH 6.8; 12% SDS; 60% Glycerol; 0.12% Bromophenol Blue; 600 nM DTT), boiled for 3 min at 100 °C and proteins were separated on a 7.5% SDS–PAGE gel. After electrophoresis, proteins were transferred to a nitrocellulose membrane (Amersham) by semidry transfer system (Hoefer). Membrane was blocked with 5% non-fat dried milk in TBST (50 mM Tris pH 7.5; 150 mM NaCl, 0.05% Tween-20) for 1 h at room temperature (RT) with mild agitation. Primary antibodies were diluted, in 1% non-fat dried milk, as follows: mouse anti-Bub3 (1:1000, 611731 clone 31, BD Biosciences); mouse anti-DIC (1:200, D5167 clone 70.1, Sigma–Aldrich); rabbit anti-Spindly (1:3000, gift from Dr. R. Gassmann, IBMC, Portugal), rabbit anti-α-tubulin (1:1500, ab15246, Abcam) and mouse anti-α-tubulin (1:5000, T568 Clone B-5-1-2, Sigma–Aldrich). After washing in TBST, membrane was probed, for 1 h at RT, with horseradish peroxidase (HRP)-conjugated secondary antibodies, diluted at 1:1500 (anti-mouse, Vector) or at 1:1000 (anti-rabbit, Sigma). Proteins were visualized using the Enhanced Chemiluminescence (ECL) method and the relative signal intensity of the bands was determined as normalized against α-tubulin intensity levels using ImageJ 1.4v software (http://rsb.info.nih.gov/ij/).

2.3. Immunofluorescence

Cells were fixed in fresh 2% paraformaldehyde (Sigma–Aldrich) in phosphate-buffered saline (PBS) for 12 min, rinsed three times 5 min in PBS and permeabilized with 0.5% Triton X-100 in PBS for 7 min. Alternatively, cells were fixed in −20 °C cold methanol for 10 min and rehydrated twice in PBS. Non-specific binding sites were blocked with 10% FBS in PBST (PBS plus 0.05% Tween-20) for 30 min at RT. Then cells were incubated for 1 h with primary antibodies diluted in PBST containing 5% FBS as follows: human anti-CREST (1:4500, gift from Dr. E. Bronze-da-Rocha, IBMC, Porto, Portugal); mouse anti-Hec1 (1:600, ab3616, Abcam); rabbit anti-Spindly (1:3000, gift from Dr. R. Gassmann, IBMC, Portugal); rabbit anti-α-Tubulin (1:100, Abcam); mouse anti-γ-Tubulin (1:1500, T6557, Clone GTU-88, Sigma–Aldrich) mouse anti-α-Tubulin (1:2500, Sigma–Aldrich). After washing in PBST, cells were incubated with secondary antibodies for 1 h. All secondary antibodies were used at 1:1500 (Molecular Probes), with the exception of Alexa Fluor 647-conjugated secondary antibody which was used at 1:2000 (Molecular Probes). DNA was stained with 2 μg/mL 4′,6-diamidino-2-phenylindole (DAPI, Sigma–Aldrich) diluted in Vectashield mounting medium (Vector, H-1000).

2.4. Functional assays for kinetochore–microtubule attachments

To assess cold-stable microtubules, cells in culture medium were incubated at 4 °C for 5 min and processed immediately for immunofluorescence with anti-α-tubulin and anti-HEC1 antibodies. Inter-kinetochore distance was measured between HEC1 spots on kinetochore pairs of bi-oriented chromosomes. kinetochore stretching (intra-kinetochore distance) was obtained by subtracting the distance between CENP-A spots (inner kinetochore marker) from the distance of HEC1 spots (outer kinetochore marker), using GFP-CENP-A expressing HeLa cell line. More than 50 kinetochore pairs from 10 cells were analyzed. To evaluate the ability of KT-MT attachments to drive chromosome congression, cells were first incubated with 1 μM nocodazole (Sigma–Aldrich) for 1 h to depolymerize microtubules, in the presence of 10 μM of the proteasome inhibitor MG-132 (Sigma–Aldrich) in order to arrest cells at metaphase-anaphase boundary. Then cells were released into medium in the presence of MG-132 for 1 h before immunostaining [10]. Nocodazole washout gives cells the opportunity to nucleate a new set of microtubules and MG132 give chromosomes time to achieve successful bipolar KT-MT attachments and to align at the equator to (re)organize a metaphase plate. More than 750 mitotic cells were counted for each condition.

2.5. Image acquisition and processing

Phase-contrast images were acquired with a 10× objective, on a Nikon TE 2000U microscope, using a DXM1200F digital camera and with Nikon ACT-1 software (Melville, NY). Fluorescence images were acquired with Plan Apochromatic 63×/NA 1.4 objective on an Axio Observer Z.1 SD microscope, coupled to an AxioCam MR3 digital camera (Carl Zeiss, Germany). Z-stacks were acquired at 0.4-μm intervals and images were processed using ImageJ software after deconvolution with AxioVision Release 4.8.2 SPC software. Insets are representative of each condition with 2–4 stacks projection.

Quantification of kinetochore fluorescence signals was performed as previously described except that values were normalized to Hec1 fluorescence intensities [10]. Each value was derived from at least 300 kinetochores in ten representative cells. For quantification of cold-stable microtubules, unattached and attached kinetochores were counted in 5 representative cells as previously described except that Hec1 staining was used to identify kinetochores in image Z-stacks [10]. More than 90 kinetochores were counted per cell.

2.6. Statistical analysis

Data are presented as the means ± standard deviation (S.D.) of at least three independent experiments. Statistical analysis was performed using an unpaired Student *t*-test in GraphPad Prism version 6 (GraphPad software Inc., CA, USA). The level of significance was set at probabilities of $^{*}P < 0.05$, $^{**}P < 0.01$, $^{***}P < 0.001$ and $^{****}P < 0.0001$.

3. Results and discussion

3.1. Bub3 and dynein are not mutually interdependent for kinetochore localization

To study the relationship between Bub3 and dynein in KT-MT attachment, we performed single and double depletions using

validated siRNAs (Fig. 1A and B). An important question that needed to be clarified first was whether depletion of one protein affects kinetochore localization of the other. This possibility was excluded as Bub3 properly localized to kinetochores in dynein-depleted cells, as did dynein in Bub3-depleted cells (Fig. 1B). Thus, the chromosome misalignment phenotype known to result from depletion of one protein is not a consequence of depletion of the other.

3.2. Dynein depletion partially suppresses chromosome misalignment phenotype associated with Bub3 depletion

We then proceeded to the analysis of chromosome congression in the absence of both Bub3 and dynein in order to determine if a relationship exists between the two proteins. For that, we determined the ability of chromosomes to align at spindle midzone and to form a defined metaphase plate in Bub3/dynein co-depleted cells. Cells were treated with the anaphase inhibitor MG132 prior to immunostaining in order to give chromosomes enough time to reach the metaphase plate [3,10,11]. Most mitotic cells in control were blocked in metaphase (91 ± 0.7%) and had all chromosomes aligned (Fig. 2A and B). In contrast, the majority of mitotic Bub3-depleted cells (62 ± 1.5%) that reached metaphase exhibited misaligned chromosomes (Fig. 2A and B), consistent with defective KT-MT attachments we previously reported [10]. In dynein-depleted cells, we observed three distinct mitotic figures: metaphases with misaligned chromosomes (36.2 ± 7.2%), full metaphases (26.2 ± 3.1%), and mitotic cells with no defined organization that we scored as disorganized metaphases (37.6 ± 2.4%) (Fig. 2A and B). While the presence of metaphases with misaligned chromosomes reflects the dynein role in initial attachments and probably in their conversion into end-on attachment [7,12,13], the disorganized figures displayed abnormal mitotic spindle morphology with no focused spindle poles, probably reflecting dynein role in spindle organization and centrosomes separation [14,15]. Nevertheless, the metaphases with misaligned chromosomes and full metaphases showed bipolar spindles with focused poles as judged by the centrosome marker γ-tubulin (Fig. 2C). Quantification of metaphases in MG132-treated Bub3/dynein co-depleted cells showed a significant increase in full metaphases, from 38.4 ± 1.5% in Bub3- and 26.2 ± 3.1% in dynein-depleted to 47.4 ± 8.1% after depletion of both proteins (Fig. 2A and B). This increase was accompanied with a concomitant decrease in metaphase with misaligned chromosomes, with a drop from 61.7 ± 1.5% in Bub3 and 36.2 ± 4.6% in dynein single knockdown to 22.4 ± 1.8% in the absence of both proteins. The percentage of disorganized metaphases did not seem to be affected by the co-depletion.

Then, we sought to clarify whether the contribution of dynein to the rescue of chromosome alignment observed in Bub3/dynein co-depletion was specific to its kinetochore pool, or it is due to the multiple roles of its cytosolic pool in mitotic spindle organization. To selectively deplete dynein from kinetochore, we used validated siRNAs against Spindly, a protein required for dynein recruitment

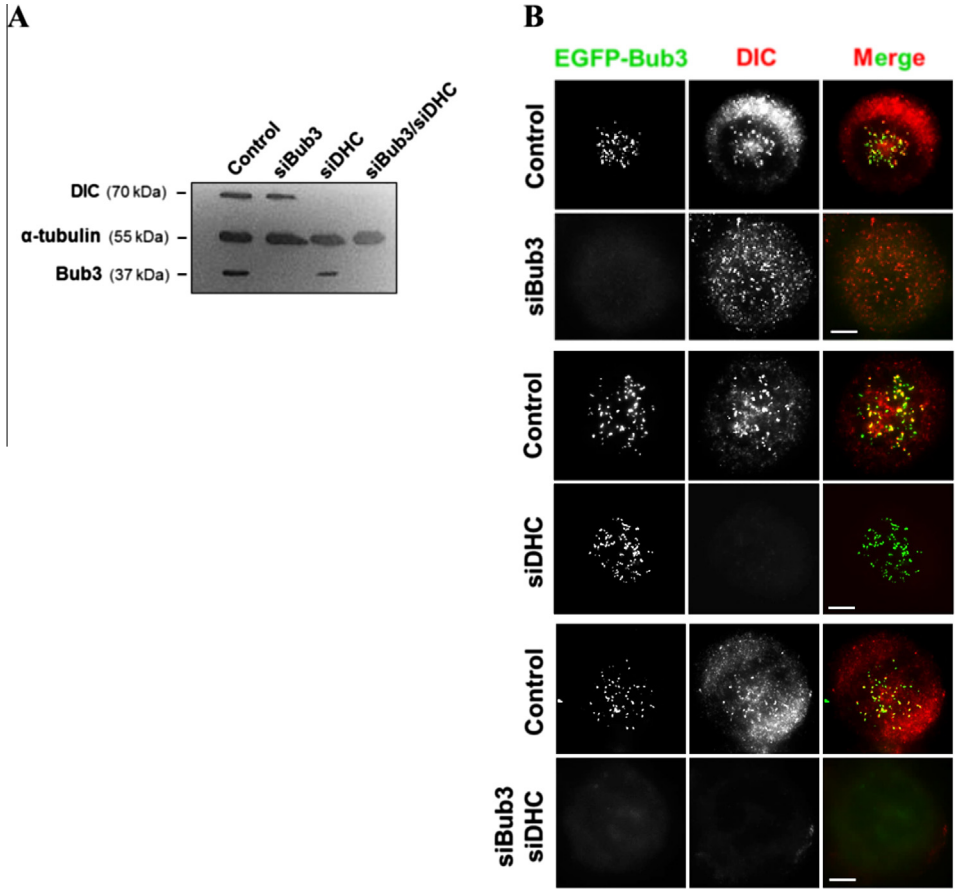

Fig. 1. Bub3 and dynein depletion are not interdependent for kinetochore localization. (A) Immunoblots showing efficient siRNA-mediated individual (siBub3 and siDHC) and co-depletion of Bub3 and dynein (siBub3/siDHC). Note that the levels of one protein is not affected by depletion of the other. (B) Immunofluorescence images showing that (top panel) depletion of Bub3 (siBub3) did not affect kinetochore localization of dynein (DIC), and (middle panel) depletion of dynein (siDHC) did not affect kinetochore localization of Bub3 (EGFP-Bub3); (bottom panel) shows depletion of both proteins (siBub3siDHC). Cells were treated with 1 μM nocodazole prior immunofluorescence to create conditions where Bub3 and dynein are maximally enriched at kinetochores. Bar, 5 μm.

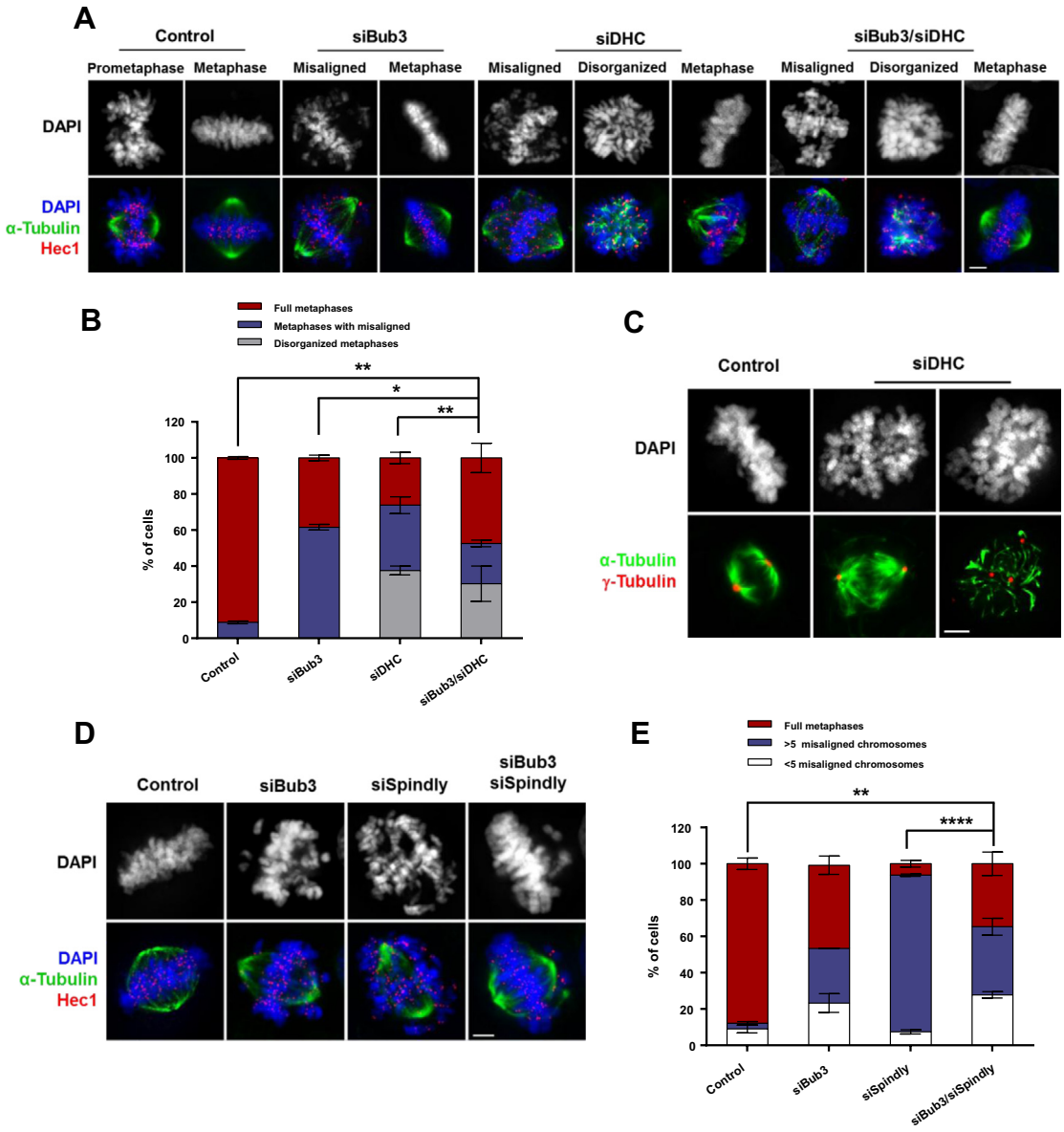

Fig. 2. Bub3 and dynein co-depletion rescues chromosome alignment. (A) Immunofluorescence images showing misalignment phenotype after individual (siBub3 and siDHC) and co-depletion of Bub3 and dynein (siBub3/siDHC). Microtubules (green) were stained with anti-α-tubulin antibody, kinetochores (red) with anti-Hec1 antibody, and DNA (blue) with DAPI. (B) Quantification of data shown in (A). (C) Immunofluorescence images of control and siDHC-treated cells, stained for α-tubulin to visualize spindle microtubules (green) and for γ-tubulin to localize spindle pole position (red). In siDHC cells, metaphase plates with misaligned chromosomes (middle) exhibited a defined bipolar spindle similar to control (left), while disorganized metaphases (right) displayed abnormal spindle morphology and thus were excluded from this study. (D) Immunofluorescence images showing many misaligned chromosomes in a cell depleted of Bub3 (siBub3) or Spindly (siSpindly). Co-depletion (siBub3/siSpindly) greatly improved chromosome alignment. Cells were processed as in (A). (E) Quantification of data shown in (D). $^{*}P < 0.05$, $^{**}P < 0.01$, $^{***}P < 0.001$ and $^{****}P < 0.0001$. Bar, 5 μm.

to kinetochores [16]. As expected, dynein was absent from kinetochore after Spindly depletion (Supplementary Fig. 1A and B). We also certified that Bub3 and Spindly were not interdependent for kinetochore localization (Supplementary Fig. 1C and D). In MG132-treated Bub3/Spindly co-depleted cells, the severity of chromosome misalignment was clearly attenuated, compared to Spindly depletion, with a net increase in well-defined metaphase plates having few to no misaligned chromosomes (Fig. 2D and E). Collectively, these observations indicate that co-depletion of Bub3 and dynein suppresses, at least partially, the misalignment phenotype generated by depletion of each protein individually, which probably underlies an antagonistic interaction. Of note, as a dynein-recruitment independent role in chromosome alignment has been proposed for Spindly [17], we do not exclude the possibility that Bub3/Spindly co-depletion is also rescuing alignment defects that are not necessarily dependent on dynein.

3.3. Kinetochore–microtubule attachments in Bub3/dynein co-depleted cells are stable and functional enough to restore the alignment

Successful chromosome congression relies on stable and functional KT-MT attachments. We asked whether the apparent rescue of chromosome alignment upon Bub3/dynein depletion was due to a rescue of stable and functional KT-MT attachments. For that, we performed functional assays to test the robustness of KT-MT attachments and their ability to generate tension and to drive chromosome movement and alignment in co-depleted cells.

The robustness of kinetochore-attached microtubules (or K-fibers) was tested after a brief exposure of cells to low temperature. Low temperature induces disassembly of unstable, but not stable, K-fibers [18]. After cold treatment, metaphases in Bub3- or dynein-depleted cells exhibited few cold-resistant K-fibers and many unattached kinetochores, as judged by Hec1/tubulin immunostaining (Fig. 3A). Instead, unattached kinetochores were rather rare or absent in metaphases of co-depleted cells, almost indistinguishably from control metaphases, indicating that robust KT-MT connections were restored.

Robustness of KT-MT attachments in co-depleted cells was further assessed for their ability to generate tension across sister-kinetochores due to poleward forces exerted by microtubules on kinetochores. Tension between kinetochores can be appreciated by measuring inter- and intra-kinetochore distances [19]. Inter-kinetochore distance reflects centromere stretching and intra-kinetochore distance reflects stretching at the kinetochore itself [20,21]. Inter-kinetochore distance was found to be smaller in siBub3 cells (1.39 ± 0.09 μm) and in siDHC cells (1.56 ± 0.10 μm), compared to control cells (2.08 ± 0.37 μm), in agreement with previous data (Fig. 3B) [3,7,22]. In co-depleted cells, inter-kinetochore distance slightly increased to reach 1.66 ± 0.19 μm. Although it did not reach control values, this slight increase underlies an improvement in KT-MT attachments. Interestingly, a clear improvement of

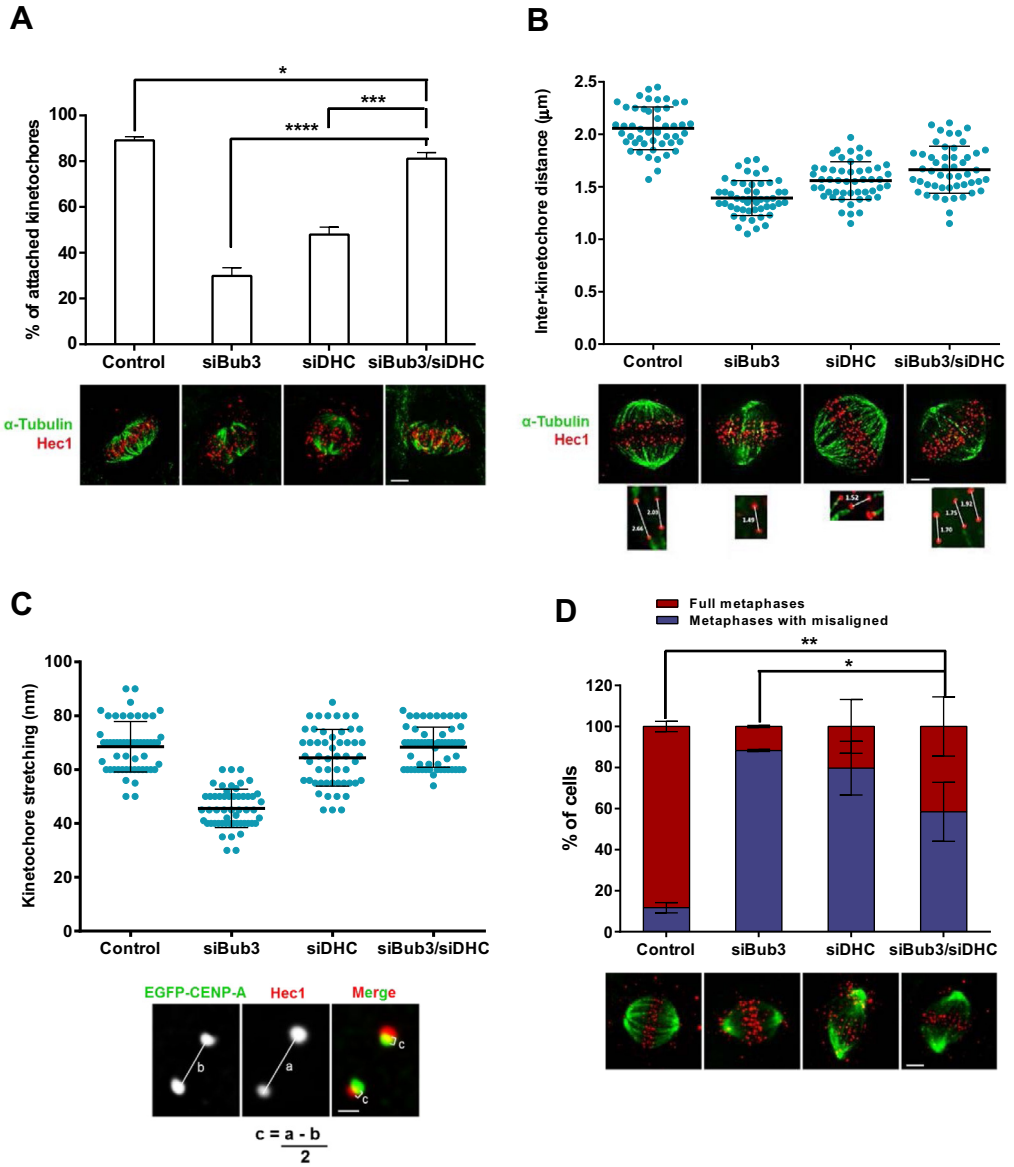

Fig. 3. Bub3 and dynein co-depletion rescues stable and functional Kinetochore–microtubule attachments. (A) (Top) Quantification of cold-stable microtubules (as percentage of attached kinetochores per cell) after individual (siBub3 and siDHC) and co-depletion of Bub3 and dynein (siBub3/siDHC). (Bottom) Representative immunofluorescence images of (A) showing several unattached kinetochores (free Hec1 red spots) in cells depleted of Bub3 (siBub3) or dynein (siDHC), whereas most kinetochores were attached (Hec1 red spots with attached green fibers) in siBub3/siDHC cells, similarly to control. (B) Distance between Hec1 spots of aligned sister kinetochore pairs, showing a slight increase in inter-kinetochore distance in siBub3/siDHC cells, comparatively to individual depletions. Lower images and insets are representative of each condition. (C) Kinetochore stretching (intra-kinetochore distance), of bi-oriented kinetochores, showing an increase in intra-kinetochore distance in siBub3/siDHC, comparatively to individual depletions. Kinetochore stretching (c) was measured by subtracting the distance between inner kinetochore CENP-A spots (b) from that between outer kinetochore Hec1 spots (a) and divided by two, as illustrated in the lower image. (D) Cells were treated with nocodazole to depolymerize microtubules in the presence of MG132, released into fresh culture medium containing MG132 for 45 min, and stained for α-tubulin (green) and Hec1 (red). The ability of cells to form a metaphase plate was significantly improved in siBub3/siDHC cells, comparatively to siBub3 cells. $^{*}P < 0.05$, $^{**}P < 0.01$, $^{***}P < 0.001$ and $^{****}P < 0.0001$. Bar in (A)–(C), 5 μm; bar in (D), 1 μm.

intra-kinetochore distance (kinetochore stretching) was found in co-depleted cells (68.33 ± 0.02 nm), compared to Bub3-depleted cells (45.00 ± 0.07 nm) (Fig. 3C). Here, intra-kinetochore stretching was restored to levels indistinguishable from control (68.50 ± 0.05 nm). Intra-kinetochore stretch can occur at low levels of inter-kinetochore stretch and reflects the attachment of dynamic microtubules, ultimately leading to satisfaction of the SAC [20]. Taken together, these observations strongly indicate that Bub3 and dynein co-depletion restores robust and dynamic KT-MT attachments that are able to generate tension.

Finally, we were concerned whether the restored KT-MT attachments in co-depleted cells were functional and, thus, able to drive chromosome congression. For that, we assessed their ability to drive chromosome movement and alignment after a nocodazole treatment/washout assay in the presence of MG132. After 45 min of recovery, up to 80% of mitotic control cells have formed full metaphases, while only 12% in Bub3- and 20% in dynein-depleted mitotic cells exhibited full alignment (Fig. 3D). However, upon co-depletion, up to 40% of mitotic cells reaching full metaphases, indicating that Bub3/dynein co-depletion restores functional KT-MT attachments that are able to drive chromosome congression.

3.4. How to explain this unexpected antagonistic interaction between Bub3 and dynein and what would be its functional significance?

At first glance, the question may seem difficult to answer. Indeed, given the role of Bub3, and most probably also of dynein, in promoting end-on attachments, one should expect a rather worst chromosome misalignment phenotype in the absence of both proteins. Nevertheless, in light of previous reports, involvement of dynein in intriguing antagonistic relationships is not too surprising. For instance, depletion of dynein restored bipolar spindles in cells depleted of the drosophila homolog of human CLASP, a protein required to incorporate tubulin subunits into microtubule plus-ends, suggesting an unexpected antagonistic role of the two proteins in kinetochore–microtubule plus-end dynamics [23]. Similarly, depletion of the drosophila motor protein CENP-E partially suppressed the unstable KT-MT attachments associated with the depletion of the SAC protein BubR1 [24]. As both proteins are implicated in stable KT-MT attachments, the restoration of stable attachments upon their co-depletion revealed, again, an intriguing antagonistic interaction. Interestingly, alleviation of chromosome alignment defects has been also surprisingly seen upon co-depletion of Spindly and Rod/ZW10/Zwilch (RZZ) complex by allowing constitutive binding of Ndc80 complex to microtubules [25].

One possible explanation for the antagonistic interaction is that Bub3 and dynein are functioning in parallel pathways to promote KT-MT attachments and that the two pathways might, either directly or indirectly, mutually restrain the activity of each other. Particularly consistent with this possibility is the partial suppression of the misalignment phenotype associated with Bub3 depletion when dynein was also removed. The restoration of full metaphase after the double knockdown could result from a restoration of balance between residual Bub3/dynein or from other regulators of KT-MT interactions.

As to the functional significance of this antagonistic interaction, first we believe that this crosstalk is the result of direct interactions between Bub3 and dynein as both proteins were reported to interact in human [5]. The crosstalk between Bub3 and dynein activities may serve to fine-tune KT-MT interactions, probably to achieve optimal end-on attachments. It may also serve to link the state of KT attachment to the SAC signaling machinery in order to ensure that efficient KT-MT attachments are established before anaphase resumes. Additionally, the crosstalk would allow dynein to probe when SAC proteins need to be transported away from kinetochores to promote SAC silencing. In this respect, Bub3 itself is a dynein cargo during the step of SAC silencing according to our previous report [8]. Future work will be needed to understand the mechanistic aspect of this crosstalk.

Conflicts of interest

No potential conflicts of interest are disclosed.

Acknowledgments

This work was supported by Grants from CESPU (02-GCQF-CICS-2011N; CheckTax-CESPU-2014) and from FCT – Fundação para a Ciência e a Tecnologia under the project CEQUIMED-PEst-OE/SAU/UI4040/2014; Patrícia M.A. Silva is a PhD fellowship holder from FCT (SFRH/BD/90744/2012). We thank both anonymous Reviewers for their comments and constructive criticism.

Appendix A. Supplementary data

Supplementary data associated with this article can be found, in the online version, at http://dx.doi.org/10.1016/j.febslet.2015.10.017.

References

[1] Silva, P., Barbosa, J., Nascimento, A.V., Faria, J., Reis, R. and Bousbaa, H. (2011) Monitoring the fidelity of mitotic chromosome segregation by the spindle assembly checkpoint. Cell Prolif. 44, 391–400.
[2] Musacchio, A. and Salmon, E.D. (2007) The spindle-assembly checkpoint in space and time. Nat. Rev. Mol. Cell Biol. 8, 379–393.
[3] Logarinho, E. and Bousbaa, H. (2008) Kinetochore–microtubule interactions "in check" by Bub1, Bub3 and BubR1: The dual task of attaching and signalling. Cell Cycle 7, 1763–1768.
[4] Efimov, V.P. and Morris, N.R. (1998) A screen for dynein synthetic lethals in *Aspergillus nidulans* identifies spindle assembly checkpoint genes and other genes involved in mitosis. Genetics 149, 101–116.
[5] Lo, K.W., Kogoy, J.M. and Pfister, K.K. (2007) The DYNLT3 light chain directly links cytoplasmic dynein to a spindle checkpoint protein, Bub3. J. Biol. Chem. 282, 11205–11212.
[6] Stehman, S.A., Chen, Y., McKenney, R.J. and Vallee, R.B. (2007) NudE and NudEL are required for mitotic progression and are involved in dynein recruitment to kinetochores. J. Cell Biol. 178, 583–594.
[7] Varma, D., Monzo, P., Stehman, S.A. and Vallee, R.B. (2008) Direct role of dynein motor in stable kinetochore–microtubule attachment, orientation, and alignment. J. Cell Biol. 182, 1045–1054.
[8] Silva, P.M., Reis, R.M., Bolanos-Garcia, V.M., Florindo, C., Tavares, A.A. and Bousbaa, H. (2014) Dynein-dependent transport of spindle assembly checkpoint proteins off kinetochores toward spindle poles. FEBS Lett. 588, 3265–3273.
[9] Gassmann, R., Holland, A.J., Varma, D., Wan, X., Çivril, F., Cleveland, D.W., Oegema, K., Salmon, E.D. and Desai, A. (2010) Removal of Spindly from microtubule-attached kinetochores controls spindle checkpoint silencing in human cells. Genes Dev. 24, 957–971.
[10] Logarinho, E., Resende, T., Torres, C. and Bousbaa, H. (2008) The human spindle assembly checkpoint protein Bub3 is required for the establishment of efficient kinetochore–microtubule attachments. Mol. Biol. Cell 19, 1798–1813.
[11] Kops, G.J., Foltz, D.R. and Cleveland, D.W. (2004) Lethality to human cancer cells through massive chromosome loss by inhibition of the mitotic checkpoint. Proc. Natl. Acad. Sci. U.S.A. 101, 8699–8704.
[12] Pfarr, C.M., Coue, M., Grissom, P.M., Hays, T.S., Porter, M.E. and McIntosh, J.R. (1990) Cytoplasmic dynein is localized to kinetochores during mitosis. Nature 345, 263–265.
[13] Steuer, E.R., Wordeman, L., Schroer, T.A. and Sheetz, M.P. (1990) Localization of cytoplasmic dynein to mitotic spindles and kinetochores. Nature 345, 266–268.
[14] Vaisberg, E.A., Koonce, M.P. and McIntosh, J.R. (1993) Cytoplasmic dynein plays a role in mammalian mitotic spindle formation. J. Cell Biol. 123, 849–858.
[15] Sharp, D.J., Rogers, G.C. and Scholey, J.M. (2000) Cytoplasmic dynein is required for poleward chromosome movement during mitosis in Drosophila embryos. Nat. Cell Biol. 2, 922–930.
[16] Gassmann, R., Essex, A., Hu, J.S., Maddox, P.S., Motegi, F., Sugimoto, A., O'Rourke, S.M., Bowerman, B., McLeod, I., Yates 3rd, J.R., Oegema, K., Cheeseman, I.M. and Desai, A. (2008) A new mechanism controlling kinetochore–microtubule interactions revealed by comparison of two dynein-targeting components: SPDL-1 and the Rod/Zwilch/Zw10 complex. Genes Dev. 22, 2385–2399.

[17] Gassmann, R., Holland, A.J., Varma, D., Wan, X., Civril, F., Cleveland, D.W., Oegema, K., Salmon, E.D. and Desai, A. (2010) Removal of Spindly from microtubule-attached kinetochores controls spindle checkpoint silencing in human cells. Genes Dev. 24, 957–971.
[18] Rieder, C.L. (1981) The structure of the cold-stable kinetochore fiber in metaphase PtK1 cells. Chromosoma 84, 145–158.
[19] Waters, J.C., Skibbens, R.V. and Salmon, E.D. (1996) Oscillating mitotic newt lung cell kinetochores are, on average, under tension and rarely push. J. Cell Sci. 109 (Pt 12), 2823–2831.
[20] Maresca, T.J. and Salmon, E.D. (2009) Intrakinetochore stretch is associated with changes in kinetochore phosphorylation and spindle assembly checkpoint activity. J. Cell Biol. 184, 373–381.
[21] Uchida, K.S., Takagaki, K., Kumada, K., Hirayama, Y., Noda, T. and Hirota, T. (2009) Kinetochore stretching inactivates the spindle assembly checkpoint. J. Cell Biol. 184, 383–390.
[22] Yang, Z., Tulu, U.S., Wadsworth, P. and Rieder, C.L. (2007) Kinetochore dynein is required for chromosome motion and congression independent of the spindle checkpoint. Curr. Biol. 17, 973–980.
[23] Reis, R., Feijao, T., Gouveia, S., Pereira, A.J., Matos, I., Sampaio, P., Maiato, H. and Sunkel, C.E. (2009) Dynein and mast/orbit/CLASP have antagonistic roles in regulating kinetochore–microtubule plus-end dynamics. J. Cell Sci. 122, 2543–2553.
[24] Maia, A.F., Lopes, C.S. and Sunkel, C.E. (2007) BubR1 and CENP-E have antagonistic effects upon the stability of microtubule-kinetochore attachments in Drosophila S2 cell mitosis. Cell Cycle 6, 1367–1378.
[25] Barisic, M., Sohm, B., Mikolcevic, P., Wandke, C., Rauch, V., Ringer, T., Hess, M., Bonn, G. and Geley, S. (2010) Spindly/CCDC99 is required for efficient chromosome congression and mitotic checkpoint regulation. Mol. Biol. Cell 21, 1968–1981.